Immunodeficiencies and autoimmunity

Clinical

Research Article

Healthy preterm newborns: Altered innate immunity and impaired monocyte function

Sara De Biasi[#1] 🆔, Anita Neroni[#1], Milena Nasi[2], Domenico Lo Tartaro[1],
Rebecca Borella[1], Lara Gibellini[1], Laura Lucaccioni[1], Emma Bertucci[1],
Licia Lugli[1], Francesca Miselli[1], Luca Bedetti[1], Isabella Neri[1],
Fabrizio Ferrari[1], Fabio Facchinetti[1], Alberto Berardi[1]
and Andrea Cossarizza[1,3] 🆔

[1] Department of Medical and Surgical Sciences for Children & Adults, University of Modena
and Reggio Emilia, Modena, Italy

[2] Department of Surgery, Medicine, Dentistry and Morphological Sciences, University of
Modena and Reggio Emilia, Modena, Italy

[3] National Institute for Cardiovascular Research, Bologna, Italy

Birth prior to 37 completed weeks of gestation is referred to as preterm (PT). Premature newborns are at increased risk of developing infections as neonatal immunity is a developing structure. Monocytes, which are key players after birth, activate inflammasomes. Investigations into the identification of innate immune profiles in premature compared to full-term infants are limited. Our research includes the investigation of monocytes and NK cells, gene expression, and plasma cytokine levels to investigate any potential differences among a cohort of 68 healthy PT and full-term infants. According to high-dimensional flow cytometry, PT infants have higher proportions of CD56$^{+/-}$CD16$^+$NK cells and immature monocytes, and lower proportions of classical monocytes. Gene expression revealed lower proportions of inflammasome activation after in vitro monocyte stimulation and the quantification of plasma cytokine levels expressed higher concentrations of alarmin S100A8. Our findings suggest that PT newborns have altered innate immunity and monocyte functional impairment, and pro-inflammatory plasmatic profile. This may explain PT infants' increased susceptibility to infectious disease and should pave the way for novel therapeutic strategies and clinical interventions.

Keywords: Cytokines · Inflammasomes · Inflammation · Monocytes · Preterm births

🖥 Additional supporting information may be found online in the Supporting Information section at the end of the article.

Introduction

Preterm (PT) birth, defined as birth before 37 weeks of completed gestation, is one of the most frequent pregnancy complications.

Worldwide, PT is responsible for the mortality of more than 1 million babies annually, being the most common cause of neonatal death [1–4]. Following delivery, premature newborns are at increased risk of developing infections [1, 5–7].

Correspondence: Dr. Sara De Biasi
e-mail: sara.debiasi@unimore.it

#Both the authors contributed equally to this work.

Neonatal immunity is a developing structure that evolves gradually [8]. It mainly relies on the innate immune system, which induces a rapid, partially selective, and efficient response to different conditions [9]. Besides the presence and function of neutrophils and innate lymphoid cells, natural killer (NK) cells and monocytes play a pivotal role against infectious diseases [10]. NK cells are crucial to anti-viral immunity and are the main producers of interferon (IFN)-γ and cytotoxic proteins. Premature newborns' immune systems are characterized by lower frequencies of NK cells compared to full-term (term) newborns [11, 12].

Monocyte phenotype is influenced by the intrauterine environment. Following birth, alterations in monocyte functions may change susceptibility to additional infectious or inflammatory stimuli [12]. In full-term infants, monocytes represent 7–38% of all circulating mononuclear cells in cord blood (CB) [7]. In PT and full-term infants, monocytes show decreased expression of HLA-DR and Toll-like receptor (TLR)-4, and also display a tendency to develop a Th2-type response compared to adults [13]. According to the surface expression of CD14 and CD16 antigens, monocytes can be classified into three main subsets characterized by different functions: classical ($CD14^+CD16^-$), intermediate ($CD14^+CD16^+$), and nonclassical monocyte ($CD14^{+/-}CD16^{+/+}$). Intermediate and nonclassical types are more capable of triggering inflammatory responses [14, 15].

One of the main functions of monocytes is to recognize pathogen- or damage-associated molecular patterns (PAMPs or DAMPs, respectively) through different TLRs. Transduced signals then trigger inflammasomes, which are multimeric protein complexes. Inflammasomes activate the caspase-1 enzyme that transforms the precursors of pro-IL-1β and pro-IL-18 inflammatory cytokines into IL-1β and IL-18 effector molecules. These cytokines belong to IL-1 family and are fundamental in regulating both innate and adaptive immune responses and are crucial in host defense against infections [2, 10, 16]

In PT newborns, inflammasome component levels are increased. This increased activity possibly causes an inflammatory phenomenon that leads to abnormal fetal airway development [17–19]. Non-infectious maternal issues, including maternal metabolic syndrome, pre-eclampsia, gestational diabetes, and maternal chorioamnionitis, have also been positively correlated with PT and increased inflammasome activity in PT infants [17].

Understanding susceptibility to infectious disease in PT infants, by identifying alterations in the innate immune profile compared to full-term infants, could pave the way to novel therapeutic strategies and clinical interventions. However, an in-depth comparison between the immune cell profiles of PT and full-term infants are limited. We aim to investigate monocyte compartment and inflammasome functionality with high-dimensional flow cytometry, gene expression, and quantification of plasma cytokine levels among healthy PT and full-term infants.

Results

Characteristics of study population

A total of 68 births (68 mothers and 68 neonates) were enrolled in this study. All mothers were nulliparous. Of the 54 neonates (79%) born at term, 26 were delivered by spontaneous labor and 28 by elective cesarean section. Among the 14 PT infants (21%), six were delivered by spontaneous labor and 11 by elective cesarean section. Given the small cohort of PT infants, evaluation according to delivery method could not be ascertained (see Methods). Most women were Caucasian and mean maternal age was 33.5 ± 4.5 years. There were no differences in maternal age among PT or full-term births or according to delivery method among term deliveries. Gestational ages ranged from 31.0 to 36.1 weeks (median 34.4) for PT and 37.0–41.0 weeks (median 39.5) for term deliveries. All newborns were considered healthy, defined as no admittance to ICU and without diagnoses of respiratory failure, cardiovascular issues, or infection. Table 1 reports the main clinical and demographic characteristics of both mothers and infants.

Plasma level of alarmin S100A8 is higher in PT

The systemic level of inflammation was characterized by plasma levels of 23 soluble molecules related to monocyte functionality and immune modulation. Interleukin (IL)-4 plays a crucial role in the success of pregnancy and there is strong evidence that a deficiency in IL-4 along with an increase in Th1 cytokines (such as tumor necrosis factor [TNF]) contributes to spontaneous abortion and PT [20]. Among term neonates delivered by cesarean section, higher concentrations of TNF (compared to spontaneous labor) and IL-4 (compared to spontaneous and PT) were observed (Fig. 1A). However, plasma levels of IL-1β and IL-18, released after inflammasome activation, were similar among the three groups.

Matrix metalloproteinases (MMPs) degrade strength-giving collagens and other structural proteins of the arterial ECM. MMPs are responsible for the turnover of extra-cellular matrix components and are key to a wide range of processes, including tissue remodeling and release of biological factors. Overproduction of MMPs by monocyte/macrophages may be related to inflammatory disorders [21]. Soluble triggering receptor expressed on myeloid cell-1 (sTREM-1) is a special form of TREM-1 that can be detected in human body fluid. sTREM-1 constitutes a valid biomarker for rapid and early diagnosis of infectious diseases and inflammation [22]. Previous reports have suggested that a mechanism of sTREM-1 release is the proteolytic cleavage by MMP of the monocyte-anchored TREM-1 protein [23]. Among neonates delivered by cesarean section, higher concentrations of MMP-1 were observed compared to spontaneous labor. PT infants were

Table 1. Characteristic of the maternal and neonatal study cohort

Characteristics	Spontaneous vaginal delivery (S) N = 26	Caesarean section (C) N = 28	Premature newborn spontaneous labor (PT-S) N = 5	Premature newborn Caesarean section (PT-C) N = 9	q-Value (PT-S vs. S)	q-Value (PT-S vs. C)	q-Value (PT-C vs. S)	q-Value (PT-C vs. C)	q-Value (PT-S vs. PT-C)
Maternal									
Age (years, ± SD)[1]	32.50 ± 4.44	34.29 ± 4.84	32.00 ± 3.81	34.89 ± 3.33	ns	ns	ns	ns	ns
Ethnicity									
Caucasian[2]	19	24	3	7	ns	ns	ns	ns	ns
Others (Asian or African)[2]	7	4	2	2	ns	ns	ns	ns	ns
Comorbidity (n)	3§	8§§	0	0	ns	ns	ns	ns	ns
Neonatal									
GA (weeks ± SD)[1]	39.62 ± 0.98	38.50 ± 0.92	35.00 ± 2.24	34.11 ± 1.69	<0.0001	0.0084	<0.0001	0.0004	ns
Birth weight (g ± SD)[1]	3303.08 ± 420.61	3168.50 ± 486.89	2610.20 ± 530.42	2084.44 ± 312.73	0.0105	0.0359	<0.0001	0.0001	ns
Body length (cm, ± SD)[1]	49.92 ± 1.83	49.04 ± 2.03	47.00 ± 3.16	43.56 ± 3.28	0.0155	<0.0001	0.0008	0.0007	ns
Head circumference (cm, ± SD)[1]	34.15 ± 1.38	34.48 ± 1.42	32.40 ± 0.89	32.11 ± 0.78	0.0199	0.0076	0.0009	0.0002	ns
Apgar 1 min. (±SD)[1]	9.12 ± 0.59	8.86 ± 0.59	8.40 ± 0.89	7.67 ± 1.00	ns	ns	<0.0001	0.0007	ns
Apgar 5 min. (±SD)[1]	9.88 ± 0.33	9.93 ± 0.26	9.60 ± 0.55	9.11 ± 0.78	ns	ns	0.0005	0.03	ns

[1] Kruskal–Wallis test with Benjamini-Hochberg correction for multiple comparisons.
[2] Chi-square test.
§ Two women presented gestational diabetes and one suffered of previous transient ischemic attack.
§§ Three women presented gestational diabetes, one gestational diabetes and obesity, two gestational diabetes and autoimmune thyroid disease, one had an autoimmune thyroid disease, and one type 1 diabetes mellitus.
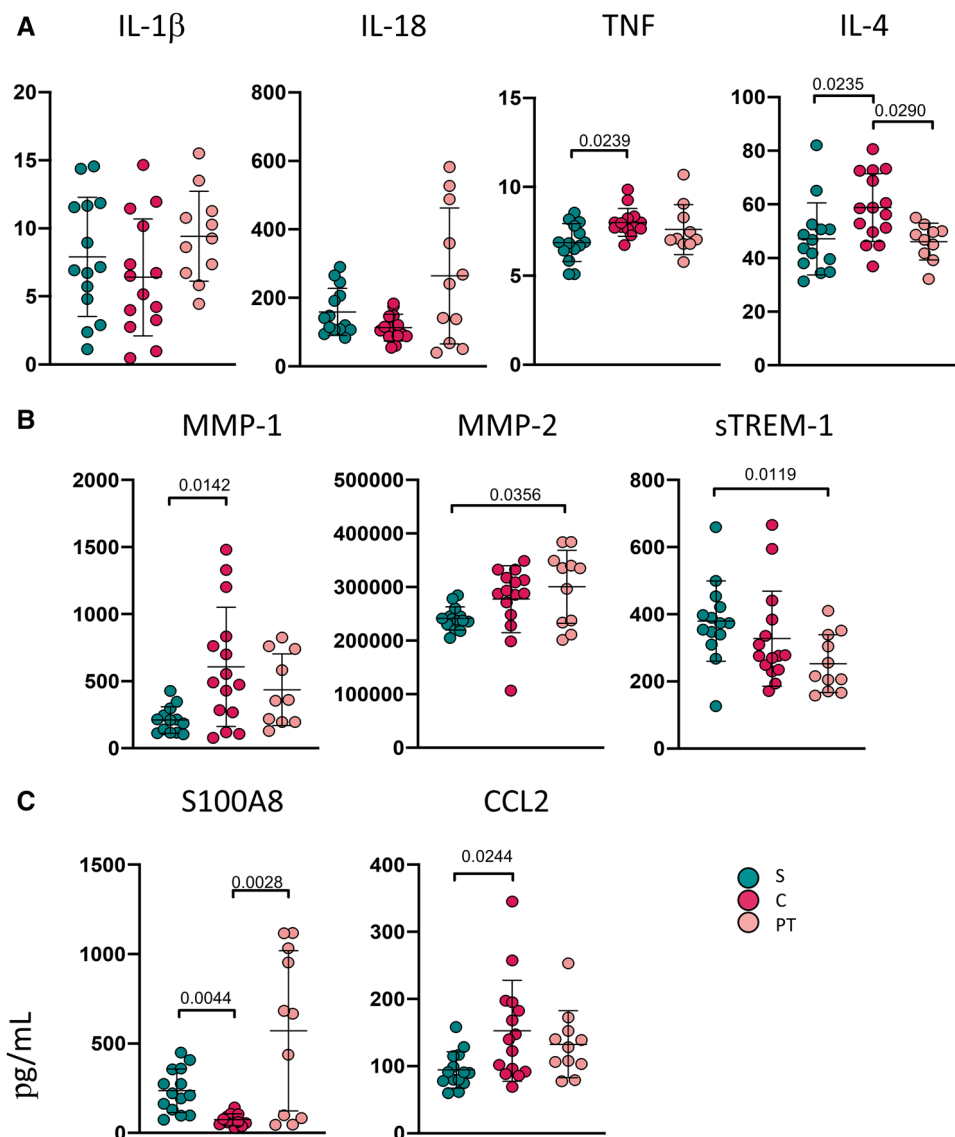All data are displayed as mean± standard deviation (SD). Ns, nonsignificant value; GA, gestational age.

Figure 1. Cord blood soluble molecules. Scatter plots of cytokines and other mediators in plasma obtained from S ($n = 14$), C ($n = 15$), and PT ($n = 11$) newborns. Scatter plots show individual values, mean ± SEM. Kruskal–Wallis test with original FDR method of Benjamini and Hochberg correction was used for the statistical analysis. Exact q-values are reported in the figure.

characterized by higher concentrations of MMP-2 and lower concentration of sTREM-1, compared to spontaneous labor (Fig. 1B).

Alarmins, also referred to as DAMPS, are endogenous molecules rapidly released into the extracellular milieu following tissue damage. Alarmin molecules are released either by active secretion from activated immune cells or passively by necrotic cells. The S100A8 protein (alarmin of the S100 family) is a calcium-binding protein expressed by monocytes. Under pathological conditions, especially in response to environmental triggers, S100A8 is induced in other cell types. Extracellular S100A8 binds to TLRs to activate the innate immune system and mediate inflammation by influencing monocyte and macrophage behavior [24]. The CCL2/CCR2 axis drives the monocyte recruitment in inflamed tissue. Cesarean section births were characterized by lower concentrations of S100A8 (compared to PT) and

lower concentrations of CCL2 (compared to spontaneous labor) (Fig. 1C). All other soluble molecules displayed similar concentrations among PT and full-term births (also according to delivery methods) (Supporting information Fig. S1).

PT infants display different proportions of CD56$^{+/-}$CD16^{+} NK cells and monocytes subpopulations

To understand whether alterations in the cytokine profile of spontaneous labor, cesarean section, and PT were associated with phenotypic alterations of the innate immunity compartment, we investigated both the basic phenotype of NK cells and monocyte phenotype by a novel 11-color flow cytometry panel. The
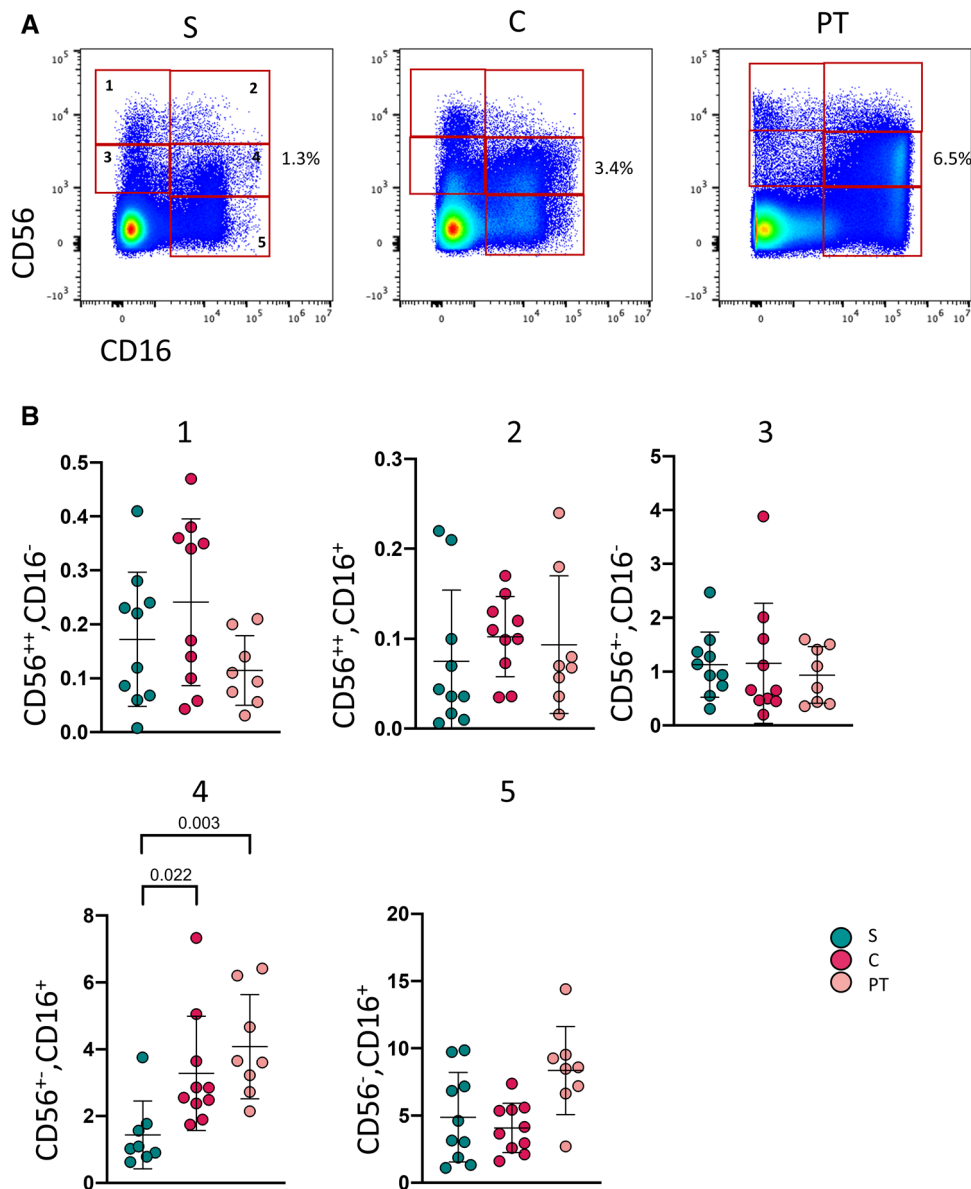
Figure 2. Analysis of natural killer (NK) cells subpopulations. (A) Representative dotplots depicting the five main subpopulations of NK subsets based on the relative expression of CD16 and CD56 in cord blood among S ($n = 10$), C ($n = 10$), and PT ($n = 8$). From left to right, it is possible to identify (1) CD56^{++}CD16$^-$, (2) CD56^{++}CD16$^{+/-}$, (3) CD56$^{+/-}$ CD16$^-$, (4) CD56$^{+/-}$ CD16$^+$, and (5) CD56$^-$ CD16$^+$. (B) Dotplots show the relative cells percentage of the five NK clusters among S ($n = 10$), C ($n = 10$), and PT ($n = 8$) newborns. The central bar represents the mean $\pm$ SEM. Kruskal–Wallis test with original FDR method of Benjamini and Hochberg correction was used, and exact q-value is shown.

expression of different receptor markers and markers related to cell activation and exhaustion were investigated. We included CD56 and CD16 for NK cells and HLA-DR, CD16, CD14, and CD13 for the analysis of classical, intermediate, and nonclassical monocytes, together with immature forms. Moreover, we investigated the expression of the chemokine receptors CX3CR1, CCR2, and CCR5. Finally, we analyzed the expression of PD-L1 and CD56 on monocytes as one readout of their function [25].

By manual gating, we analyzed NK cells, as depicted in Fig. 2A and Supporting information Fig. S2. NK cells can be divided based on the relative expression of the CD16 and CD56 surface markers. The two major subsets are CD56^{++}CD16$^{+/-}$

and CD56$^{+/-}$CD16$^+$, respectively. Five NK populations have been identified: (1) CD56^{++}CD16$^-$, (2) CD56^{++}CD16$^{+/-}$, (3) CD56$^{+/-}$CD16$^-$, (4) CD56$^{+/-}$CD16^{++}, and (5) CD56$^-$CD16^{++} [26, 27]. The CD56$^{+/-}$CD16^{++} NK population represents at least 90% of all NK cells in peripheral blood and are therefore the main circulating subset. Unlike adult peripheral blood, umbilical CB contains a significant proportion of CD56$^-$CD16$^+$ (NK population 5). NK population 5 has also been described in association with chronic viral infections, including hepatitis C, and HIV infection cells [28, 29]. NK population 5 cells have poor cytolytic ability with impaired cytokine production and are considered immature, dysfunctional, or anergic [30, 31]. Higher proportions of

$CD56^{+/-}CD16^{+}$, cytolytic and rapid producers of abundant IFN-γ upon activation, were observed among PT compared to spontaneous labor and cesarean section (Fig. 2B) [32].

In the monocyte compartment, the most immature cells expressed high levels of HLA-DR but did not express CD13 or CD14. As monocytes mature, they acquire increasing levels of CD13 and CD14, with high expressions of these molecules in mature cells. The level of HLA-DR on mature monocytic cells can vary according to the state of activation [14, 33]. To begin, we investigated the percentage of mature ($CD13^{+}CD14^{+}$) and immature ($CD13^{-}CD14^{-}$) monocyte subpopulations (Fig. 3A, Supporting information Fig. S3). PT birth was characterized by higher percentages of immature monocytes compared to spontaneous labor and cesarean section. We also observed a trend toward a higher percentage of $CD13^{-}CD14^{+}$ among PT newborns. These cells that may represent a transitional form of monocytes from immature to mature stages.

Additionally, within mature monocytes, we analyzed the percentages of classical ($CD14^{+}CD16^{-}$), intermediate ($CD14^{+}CD16^{+}$), and nonclassical monocytes ($CD14^{+/-}CD16^{+/+}$). Monocyte subsets differ according to their ability to present antigens and produce pro-inflammatory cytokines, as well as their expression of specific homing receptors. Interestingly, they can upregulate the so-called inhibitory receptors belonging to the family of immune checkpoints, such as PD-1 and its ligands (including PD-L1) [10, 14]. We found that PT was characterized by lower percentages of classical monocytes and higher proportions of intermediate monocytes, compared to spontaneous labor and cesarean section (Fig. 3B).

To better decipher the monocyte landscape and consider the complete heterogeneity of this population, we performed an unsupervised analysis of the multidimensional information obtained by FlowSOM meta-clustering. Of the 20 clusters obtained, five were filtered out as resembling NK cells (mainly, $CD16^{+}CD56^{+}$) and all lineage negative cells (Supporting information Fig. S4). The remaining 15 clusters represented different monocyte populations spanning from immature to mature forms (see the UMAP graph in Fig. 4A). Classical monocytes were mainly classified as $CD16^{-}CD13^{+}CD14^{+}HLA-DR^{+}CX3CR1^{+}CCR2^{+}$; a small cluster also expressed CCR5. A population of classical monocytes without CD13 expression, therefore resembling a population of immature monocytes, were identified as $CD14^{+/-}HLA-DR^{+/-}CX3CR1^{+/-}CCR2^{+}$. We found three clusters of intermediate monocytes: $CD16^{+/-}CD13^{+}CD14^{+}HLA-DR^{+}CX3CR1^{+}CCR2^{+}$, those also expressing CCR5 and an immature subset ($CD16^{+}CD13^{+/-}CD14^{+/-}HLA-DR^{-}$). Three nonclassical monocyte subsets were also identified: $CD16^{+/+}CD13^{+}CD14^{+/-}HLA-DR^{+}CX3CR1^{+}CCR2^{+}$, those not expressing CCR2, and their immature counterpart nonexpressing CD13. None of the nonclassical monocytes expressed CCR5, and all these clusters expressed low levels of CD56. Finally, six clusters were identified as immature forms that did not express CD14 but were $HLA-DR^{+/-}$ and $CD13^{+/-}$. Three of the six clusters expressed CCR5 or CCR2, and none of them expressed CD56 (Fig. 4B).

A diffusion map defines the differentiation trajectories of monocytes. Our analysis revealed that a population of immature monocytes (Fig. 4C, left side of the plot) gives origin to different populations of mature monocytes, which cluster in the same area of the plot (Fig. 4C, right side of the plot).

The unsupervised analysis confirmed data obtained by manual gating. Significant alterations in the proportions of different monocyte subsets were identified. When compared to spontaneous labor, PT displayed lower proportions of classical monocytes and higher percentage of cells that, even if they are $HLA-DR^{+}CD13^{-}CD14^{-}$, were detected in the electronic gate used for identifying monocytes on the basis of their physical characteristics (Fig. 4D). Low HLA-DR expression is an indicator of immunodepression and immunosuppressive phenotype. Moreover, we investigated the median fluorescence intensity (MFI, that is proportional to the amount of molecules expressed on the cell surface) of PD-L1, a marker that identifies a more suppressive phenotype and indicates a worse prognosis in sepsis and infections [34]. We found a higher expression of PD-L1 in PT classical monocytes when compared to cesarian section and spontaneous labor (Fig. 4E). Similar proportions of all other clusters were found among cesarian section, spontaneous labor, and PT (Supporting information Fig. 5).

PT monocytes express lower level of inflammasome genes after in vitro stimulation

Monocytes are endowed with the ability to activate inflammasomes. Given the phenotypical differences we observed in monocyte composition, we aimed to assess their functional capability. The relative expression of some inflammasome genes was quantified by real-time PCR in total $CD14^{+}$ monocytes after in vitro stimulation with bacterial lipopolysaccharides (LPS). The activation of the NOD- and pyrin domain containing protein 3 (NLRP3) inflammasome can depend on both PAMPS and DAMPS [35, 36]. We observed that NLRP3 expression decreases after LPS stimulation in PT group compared to spontaneous labor (Fig. 5A).

The NLR family CARD domain-containing protein 4 (NLRC4) inflammasome protects the mucosal barriers from invading bacterial pathogens [37]. We observed that *NAIP/NLRC4* expression is increased in cesarean section compared to PT (Fig. 5A). AIM2 inflammasome, triggered by cytosolic DNA, has an important role in host defense mechanism against infections [38]. The mRNA expression of *AIM2* is considerably lower in both groups of full-term infants compared to PT. *PYCARD* is the gene that encodes for the adaptor protein apoptosis-associated speck-like protein (ASC) [39] and its mRNA expression is significantly lower in spontaneous labor compared to both cesarean section and PT (Fig. 5A).

The expression of *IL-1*β mRNA is significantly higher in both groups of full-term infants compared to PT infants. A trend toward an *IL-18* mRNA abundance and the higher expression of IL-1β was observed (Fig. 5B). Comparisons among mRNA level of different inflammasomes in nonstimulated condition were performed, as reported in Supporting information Fig. S6. In PT infants,
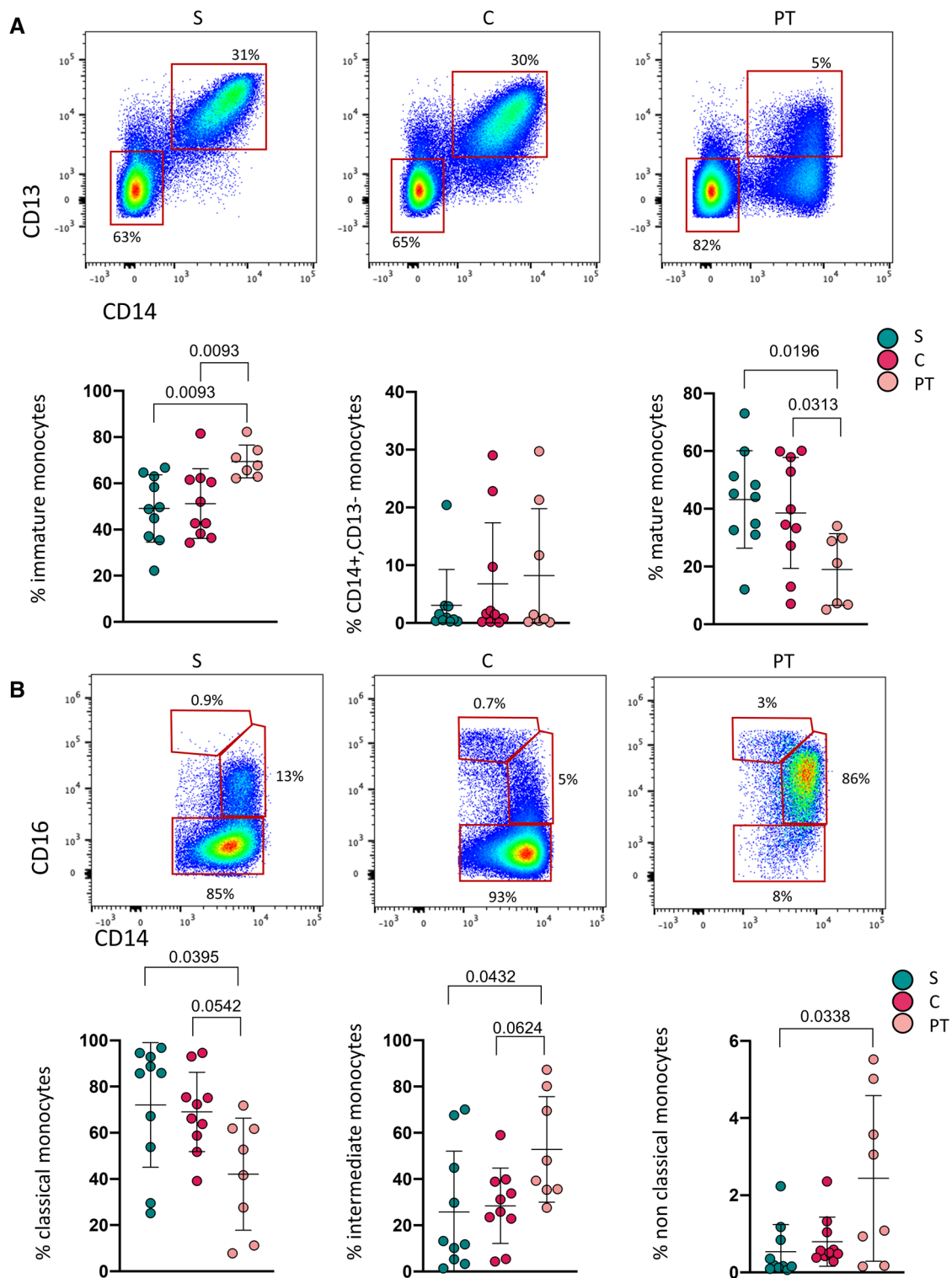
Figure 3. Analysis of monocytes subpopulations. (A) In the upper part of the figure, three representative dotplots display the percentage of mature (CD13$^+$, CD14$^+$) and immature monocytes (CD13$^-$, CD14$^-$) subpopulations among S ($n = 10$), C ($n = 10$), and PT ($n = 8$) newborn. Moreover, the percentages of immature monocytes are also shown as graph. The central bar represents the mean $\pm$ SEM. Kruskal–Wallis test with original FDR method of Benjamini and Hochberg correction was used, and exact q-value is shown. (B) Within mature monocytes, the three representative dotplots illustrate the percentages of classical (CD14$^+$, CD16$^-$), intermediate (CD14$^+$,CD16$^+$), and nonclassical monocyte (CD14$^{+/-}$, CD16$^{+/+}$). Moreover, the percentages of classical, intermediate and non-classical monocytes are also shown as graph. The central bar represents the mean $\pm$ SEM. Kruskal–Wallis test with original FDR method of Benjamini and Hochberg correction was used, and exact q-value is shown.
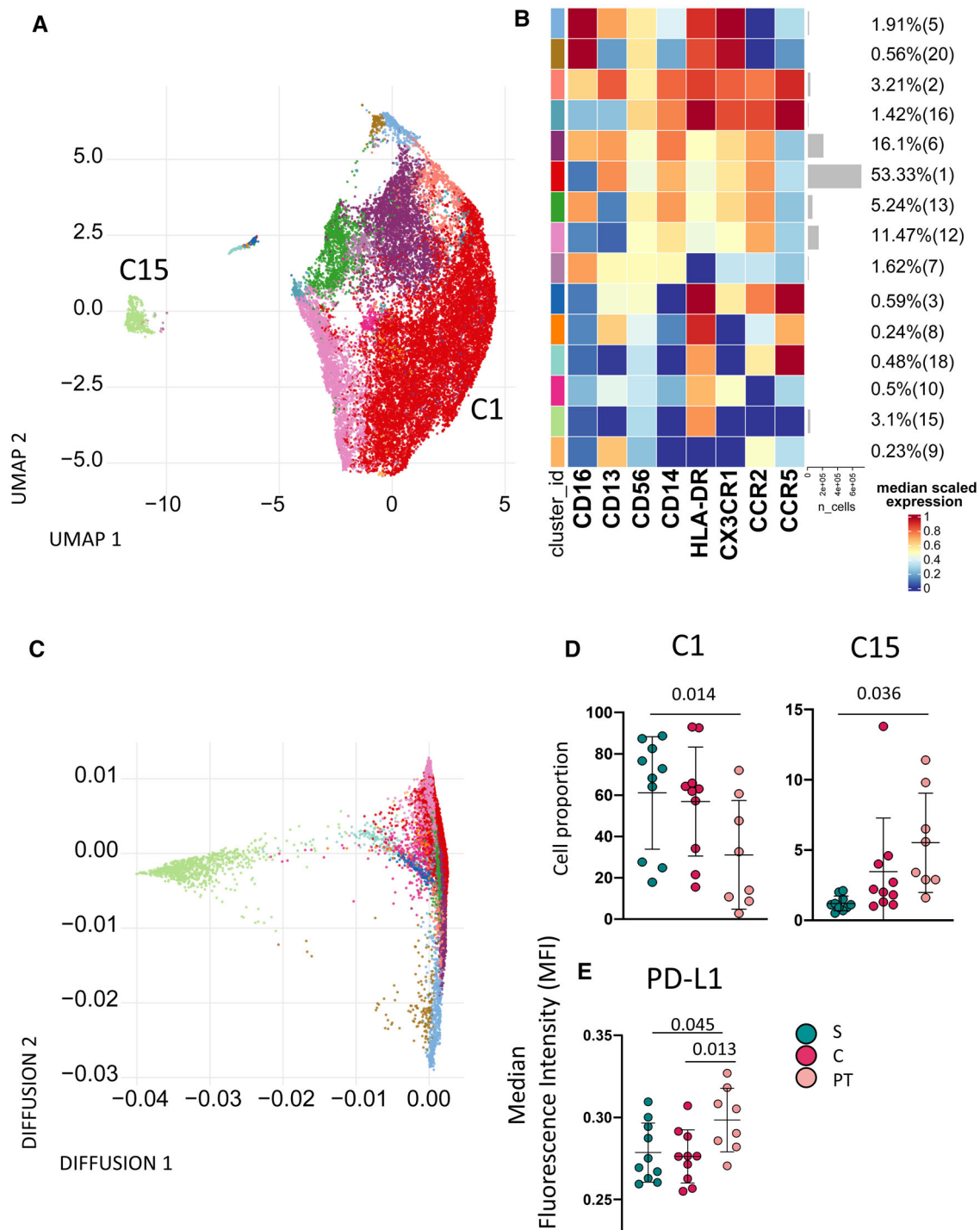
Figure 4. Cord blood monocyte landscape. (A) UMAP plot shows the 2D spatial distribution of cells from S (*n* = 10), C (*n* = 10), and PT (*n* = 8) newborns embedded with FlowSOM clusters. (B) Heatmap of the median marker intensities of the lineage markers across the cell populations obtained with FlowSOM algorithm after the manual metaclusters merging. The colors of cluster_id column correspond to the colors used to label the UMAP plot clusters. The color in the heatmap is referred to the median of the arcsinh marker expression (0 to 1 scaled) calculated over cells from all the samples. Blue represents lower expression while red represent higher expression. Light gray bar along the rows (clusters) and values in brackets indicate the relative sizes of clusters. (C) Diffusion map of monocyte differentiation based on (A). (D) Dotplots show the relative cells percentage of the two clusters among S (*n* = 10), C (*n* = 10), and PT (*n* = 8) newborns. The central bar represents the mean ± SEM. The statistical relevant adjusted *p*-values obtained by GLMM statistical test comparing S, C, and PT cluster percentages are reported in the figure. (E) Dotplot shows the surface median expression (number of molecules) of the PD-L1 on classical monocyte (C1) in S, C, and PT newborns. The C1 was selected from unsupervised analysis (shown in Fig. 2A and B). The central bar represents the mean ± SEM. Kruskal–Wallis test with original FDR method of Benjamini and Hochberg correction was used, and exact *q*-value is shown.
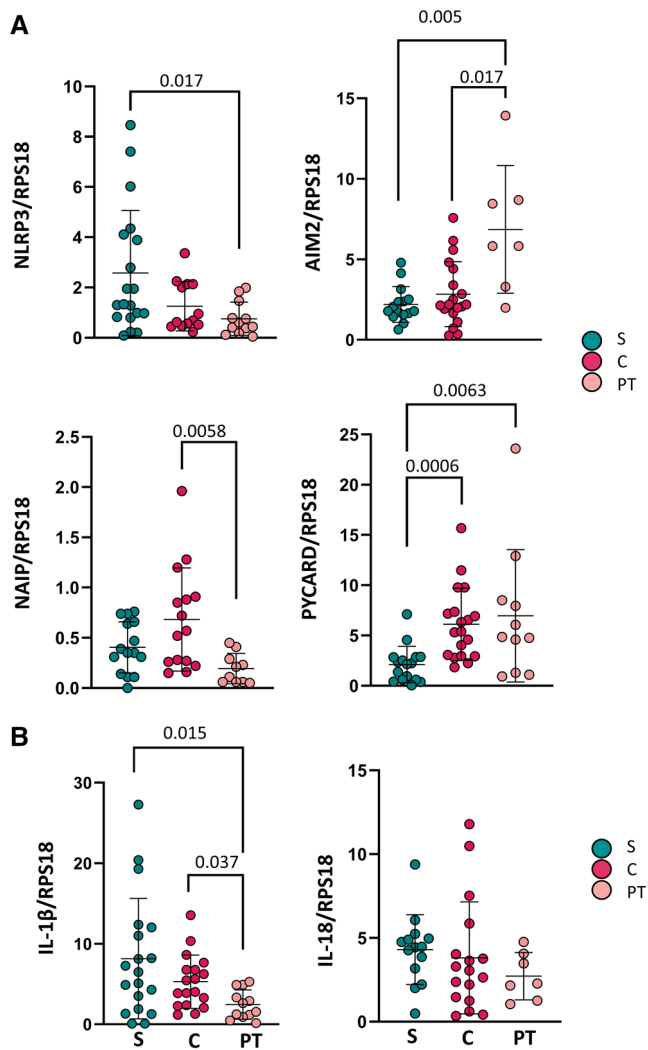
Figure 5. Inflammasome quantification after in vitro stimulation. After 2 h of LPS stimulation, changes in gene expression were evaluated versus nonstimulated monocytes and calculated through the delta-delta threshold cycle method. Kruskal–Wallis test with original FDR method of Benjamini and Hochberg correction was used to test differences among groups, and exact *q*-value is shown. Each dot represented one sample as mean value of two replicates and the central bar correspond to mean ± standard deviation (SD). Results were normalized to *RPS18* (Ribosomal Protein S18) expression for each sample. (**A**) Dotplots show the relative expression of inflammasome components such as *NLRP3*, *AIM2*, *NAIP*, and *PYCARD* gene in S (*n* = 19), C (*n* = 19), and PT (*n* = 12) newborns; six of 12 newborns were undetectable. (**B**) Relative expression of *IL-1beta* and *IL-18* genes in S (*n* = 19), C (*n* = 19), and PT (*n* = 12) newborns.

mRNA levels of *NAIP* were lower and *AIM2* were higher compared to spontaneous labor and cesarean section. mRNA levels of *PYCARD* were higher in cesarean section compared to spontaneous labor but were similar to PT. LPS stimulation effect investigations revealed that mRNA levels of *NAIP* and *PYCARD* were similar in unstimulated and LPS-stimulated conditions. Only NLRP3 inflammasome did not increase after stimulation in the PT group only, suggesting that these cells present a low capability to respond to LPS stimulus (Supporting information Fig. S7).
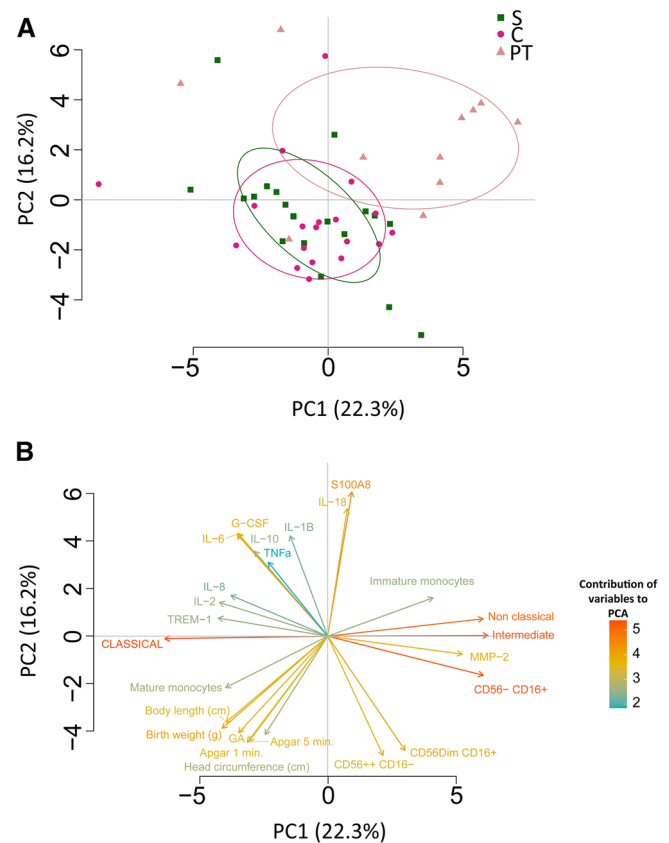

Figure 6. Principal component analysis reveals that PT group is different from C and S. (A) Principal component analysis (PCA) using the percentage of manual gated populations (NK and Monocytes) from PT, S, and C. C, purple circles (*n* = 10); S, pink squares (*n* = 10) and PT, blue triangles (*n* = 8). (B) Contribution of the different variables to PCA. The color of the arrows underlines the contribution level, while the position underlines the positive or negative contribution. Negatively correlated variables are positioned on opposite sides of the plot origin (opposed quadrants).

PCA reveals that overall PT group is different from spontaneous labor and cesarean section

Another unsupervised assay, the principal components analysis (PCA), was applied to data regarding the phenotype obtained by manual gating (NK cells and monocytes). Results revealed that PT clusters in a different position of the two-dimensional PCA space compared to spontaneous labor and cesarean section. Interestingly, spontaneous labor and cesarean section almost overlapped on the graph (Fig. 6A). Immune features related to the amount of S100A8, intermediate monocytes, and non-classical monocytes (more abundant in PT) were the main drivers of the clustering into two different areas (Fig. 6B). The same figure also indicates that spontaneous labor and cesarean section were characterized by elevated frequencies of mature and classical monocytes, and as expected, higher values of weight, length, and Apgar score at birth.
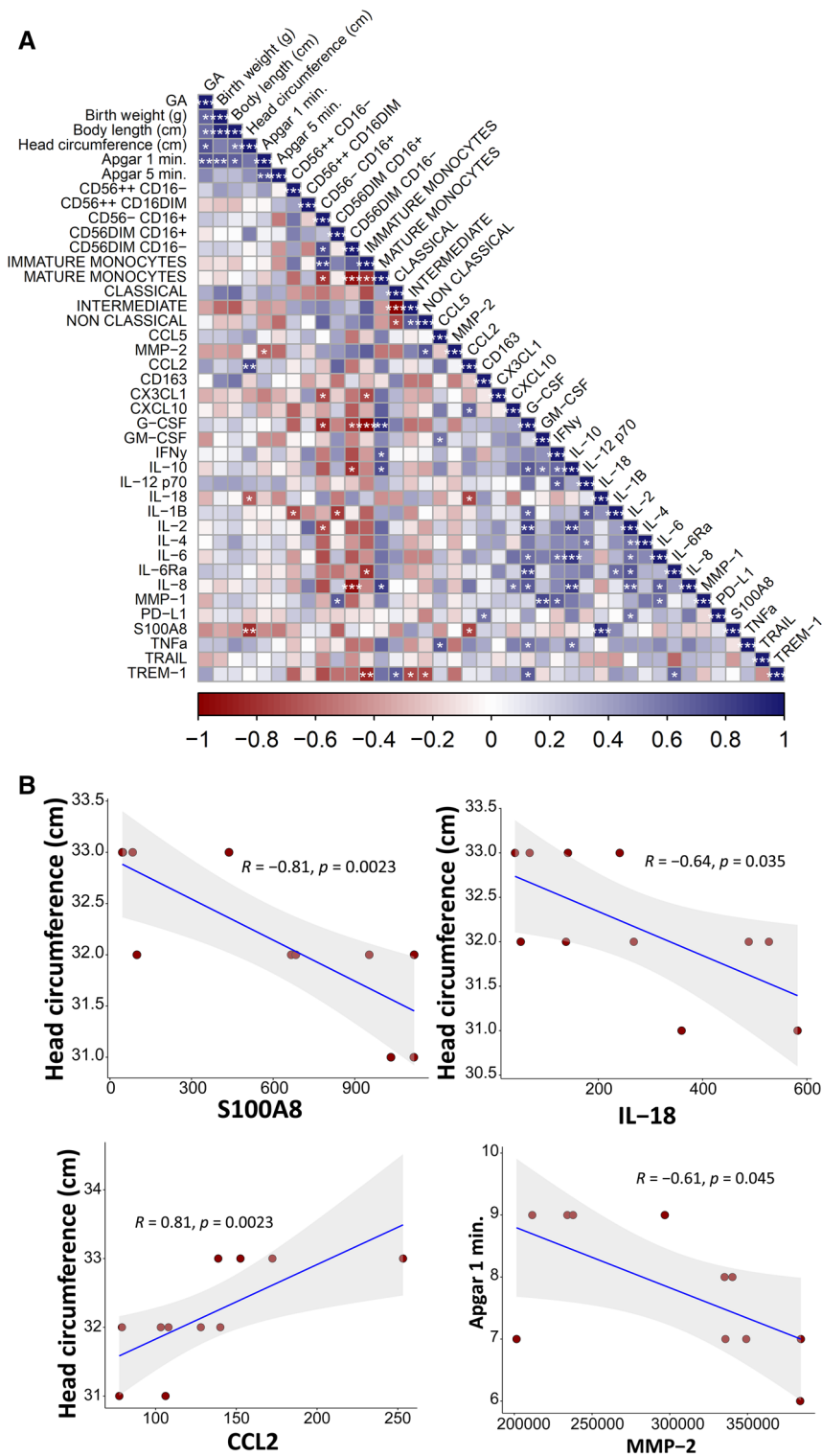
Figure 7. Correlogram showing immunological-clinical correlations in the PT group. (A) Correlogram of PT. Spearman R (ρ) values are shown from red (-1.0) to blue (1.0); specific R values are indicated by the square color. Blank fields with dots indicate lack of signal. Spearman rank two-tailed p-value was indicated by $^{*}p < 0.05$, $^{**}p < 0.01$, and $^{***}p < 0.001$. (B) Additional XY scatter plots that specifically show the relationship between the variables that are most correlated are displayed. Each scatter plot reports the regression line (blue), the Spearman R (ρ) value, the exact two-tailed p-value, and the 95% confidence bands (light gray).

Different correlations exist in PT, but not in spontaneous labor and cesarean section

We built a correlation matrix with the main clinical data, plasma levels of soluble molecules, and proportion of several cell populations (see Fig. 7 and Supporting information Figs. S8 and S9).

Of note, a highly significant inverse correlation was identified for alarmin S100A8 and head circumference in PT, but not in spontaneous labor and cesarean section. Similarly, plasma levels of the proinflammatory cytokine IL-18 inversely correlated with head circumference, suggesting that higher levels of inflammation could be associated with a small head circumference. Plasma

levels of chemokine CCL2 positively correlated with head circumference in PT, but not in spontaneous labor and cesarean section. Finally, plasma levels of MMP-2 in PT were inversely correlated with Apgar index, as measured after 1 min.

Discussion

We extensively studied and compared the innate immune landscape of PT infants compared to full-term infants. We identified significant differences not only in the proportions of innate immune cells between PT and full-term infants, but also in the pro-inflammatory plasmatic profile and monocyte functionality. PT newborns showed (i) higher plasmatic concentration of alarmin S100A8; (ii) higher proportion of NK cells with the phenotype CD56$^{+/-}$CD16^{+}; (iii) higher proportions of immature monocytes and lower proportions of classical monocytes; and (iv) lower inflammasome activation after in vitro monocyte stimulation. These differences could, at least partially, explain why PT infants are more susceptible to the development of severe infectious diseases.

Alarmins are endogenous, chemotactic, immune-activating molecules that are released as a result of cell injury or death, cell degranulation, or in response to infection. Alarmins are released from neutrophils and monocytes to initiate and amplify innate/inflammatory immune responses, inducing the activation of resident leukocytes and the production of inflammatory mediators [40]. However, in some cases, uncontrolled production of alarmins can be harmful or even fatal. S100A8/A9 is an endogenous ligand of TLR4 and can trigger multiple inflammatory pathways mediated by this receptor [41]. We found that plasmatic concentration of S100A8 was high in PT newborns and was inversely correlated with head circumference. Given that drugs, such as Paquinimod, can prevent the binding of S100A8/A9 to its receptor [42], studies are needed to ascertain whether such chemical characteristics can be of clinical use.

IL-18 is a physiological constituent of CB, and its levels increase with advancing gestational age [43]. IL-18 acts on macrophages and triggers an immune response in the chorioamniotic membranes, thereby activating the Th1 response through the release of IFN-γ by NK cells [44]. Low maternal plasma levels of IL-18 may potentially correlate with PT [45].

MMPs are involved in ECM remodeling as modulators of the tensile strength of the amnion and chorion, which are essential for maintaining a physical barrier around the fetus. Although the precise signaling pathway leading to increased expression of MMPs is not known, a potential therapeutic effect of MMP inhibition was tested directly in a murine model, resulting in a decreased rate of inflammation-mediated PT [46].

Overall, the immune landscape of PT newborns is characterized by immaturity and incapability to respond properly to different stimuli. In PT newborns, we found higher percentages of immature cells (in CB) and higher levels of PD-L1 expression (in classical monocytes). A higher expression of PD-L1 is a marker of dysfunctional activation [14]. It could be hypothesized that

such changes represent an extreme attempt to respond to external insults, likely unsuccessful in PT newborns. IL-1β mRNA levels were lower in monocytes after LPS stimulation but levels of *AIM2, PYCARD*, and *NRLP3* did not increase, compared to nonstimulated monocytes. This may indicate that monocytes are unable to induce an adequate activation of inflammasomes, with the consequent production of pro-inflammatory cytokines.

The overall characterization of the innate immune landscape in PT and full-term infants suggests that PT infants display a reduced capacity to trigger pro-inflammatory immune responses. This study adds some novel information to our understanding of the immune cell composition in PT infants and may, at least partially, explain why PT infants are more susceptible to develop severe infectious diseases. These findings may help pave the way for possible drug repositioning.

Study limitations

We are aware that our study has some limitations. The low amount of CB obtained did not allow additional immune investigations in all samples (e.g., on different populations of NK cells). Further, the small PT sample size did not enable the examination of the PT infants according to delivery method. However, data obtained in PT subjects were quite homogeneous and did not reveal any large differences. A more accurate measurement and identification of monocyte subpopulations could have been revealed by the assessment of additional markers of immature forms of monocytes and the application of a dump channel to exclude other populations expressing HLA- DR, such as B and activated T cells (that are larger and eventually more dense than other similar cells). Finally, also the quantification of different components of the inflammasome, their phosphorylation, the detection of the activation of caspase I, as well as the quantification of the release of IL-1 and IL-18 after in vitro monocyte activation could have strengthen our observations on the functionality of inflammasome.

Methods study cohort

This study was conducted in accordance with the Declaration of Helsinki and was approved by the local ethics committee (Prot# 2211/C.E.). All participants' parents signed written, informed consent. First newborns without any suspicion of infection were enrolled at the neonatal care unit of the University Hospital in Modena from October 2017 to July 2018. Exclusion criteria were (i) chromosomal abnormalities detected at prenatal investigations; (ii) major malformations detected on prenatal ultrasounds or at birth; (iii) asphyxia at birth requiring hypothermic treatment. Neonates were divided based on gestational age: <37 weeks (PT) or ≥37 weeks (term). Term infants were further subdivided according to childbirth delivery methods: spontaneous labor or elective cesarean section (cesarean section). PT births could not be evaluated according to delivery method due to

the limited number of subjects (five spontaneous labor and nine cesarean sections).

Blood sample collection, processing, and storage

CB samples were collected into ethylenediaminetetraacetic acid (EDTA) tubes. CB mononuclear cells (CBMC) were isolated by Ficoll/Isopaque density gradient centrifugation. CD14$^+$ cells were separated from CBMC through a well-standardized immunomagnetic separation technique, according to manufacturer instructions (Miltenyi Biotec, Bergisch Gladbach, Germany). Whenever possible, one aliquot of CBMC at the concentration of 5 million cells/mL was stored in liquid nitrogen in fetal bovine serum supplemented with 10% dimethyl sulfoxide.

Detection and quantification of cytokines in human plasma

Plasma was collected, centrifuged at 800 rpm for 20 min, and stored at −80°C. Plasma levels cytokines were measured in a total of 40 samples (14 S, 15 C, 11 PT) using a Luminex platform (Human Cytokine Discovery, R&D System, Minneapolis, MN). The panel included 23 cytokines: CCL2, CD163, CX3CL1, CXCL10, G-CSF, GM-CSF, IFN-γ IL-1β, IL-2, IL-4, IL-8, IL-10, IL- 12p70, IL-17, IL-18, IL-6Ra, MMP-1, PD-L1, S100A8, TNF, TRAIL, TREM-1, CCL5, and MMP-2.

Each dot represents the mean of two technical replicates.

Flow cytometry staining

CBMC isolated from CB were thawed and washed twice with RPMI 1640 supplemented with 10% fetal bovine serum and 1% each of l-glutamine, sodium pyruvate, nonessential amino acids, antibiotics, 0.1 M HEPES, 55 μM β-mercaptoethanol, and 0.02 mg/mL DNAse [47]. Then cells were washed with PBS and stained with the viability marker LIVE DEAD Aqua (Thermo Fisher Scientific). Up to 2 million cells were washed and stained at room temperature in Brilliant Stain Dye Buffer (BD Bioscience) and FACS buffer (PBS, 2% FBS) with surface mAbs anti-CD16-AF488, anti-CD13-PerCP/Cyanine5.5, anti-CD14-APC, anti-HLA-DR-AF700, anti-CX3CR1-ACP-Cy7, anti-PD-L1-PE, anti-CD56-PE-Cy7, CCR5-BV421, anti-CCR2-BV605, and, finally, 5 μL of the True-Stain Monocyte Blocker (BioLegend) was added into the antibody cocktail to reach the final staining volume of 100 μL. Supporting information Table S1 reports mAbs clones, catalog numbers, type of fluorochrome used, and mAbs dilutions. A minimum of 500,000 CBMC were acquired by using Attune NxT acoustic focusing flow cytometer (Thermo Fisher Scientific). Then all compensated .fcs files were uploaded in FlowJo software v10.7.1 and analyzed.

Representation of high-parameter flow cytometry

Flow Cytometry Standard 3.0 files were imported into FlowJo software version X (Becton Dickinson, San Josè, CA) and analyzed by standard gating to eliminate aggregates and dead cells. Then, HLA-DR$^{+/−}$ and CD14$^{+/−}$ cells were exported for further analysis in R by following a script that makes use of Bioconductor libraries and R statistical packages (CATALYST 1.10.1) [48]. The Flow-SOM platform (available at: https://bioconductor.org/packages/release/bioc/html/FlowSOM.html) was used to perform the metaclustering ($K = 25$). Data were subsequently displayed using the dimensionality reduction method named UMAP. Supporting information Figs. S10–S12 show FlowSOM clusters stratified by patients and UMAP graphs colored by the expression of markers used for clustering.

Isolation of monocytes

After cell count, monocytes were resuspended in RPMI medium, with 10% fetal bovine serum and penicillin-streptomycin (all from Thermo Fisher Scientific, Eugene, OR). At least, 1 million monocytes were plated and either stimulated, with 0.1 μg/mL LPS, or unstimulated and left for 2 h.

Real-time PCR

Total RNA was extracted from monocytes by using the Quick-RNA Miniprep kit (Zymo Research, Irvine, CA), and reverse transcription was performed using the iScript cDNA synthesis kit (Bio-Rad, Hercules, CA). Real-time quantitative PCR was performed on CFX96 Touch Real-Time PCR Detection System (Bio-Rad, Hercules, CA) using 2 μL cDNA, 2.5 μL water, 5 μL SsoAdvance Universal SYBR Green Supermix (Bio-Rad, Hercules, CA), and 0.5 μL prevalidated primer assays (Bio-Rad). The *RPS18* primer (PrimePCR Assay, Bio-Rad; identifier, qHsaCED0037454) was used as the reference gene, and *AIM2* (identifier, qHsaCID0018402), *IL1beta* (identifier, qHsaCID0022272), *IL18* (identifier, qHsaCID0006163), *NAIP* (identifier, qHsaCID0038447), *NLRP3* (identifier, qHsaCID0036694), and *PYCARD* (identifier, qHsaCED0042977) were other inflammasome genes considered. Results were normalized to *RPS18* (Ribosomal Protein S18) expression for each sample. Changes in gene expression were evaluated versus nonstimulated monocytes and calculated through the delta-delta threshold cycle method.

Principal component analysis and correlogram

Principal component analysis (PCA) was performed and visualized in R using *prcomp* and *pca3d* package. To perform PCA, we used a matrix containing the percentage of clusters for each sample based on the results of unsupervised data analysis

performed with CATALYST 1.14. The total contribution of a given variable retained by PC1 and PC2 is equal to $[(C1 * Eig1) + (C2 * Eig2)]/(Eig1 + Eig2)$, where C1 and C2 are the contributions of the variable on PC1 and PC2. Eig1 and Eig2 are the eigenvalues of PC1 and PC2.

Analysis of the correlations among all parameters

To identify possible correlations among included parameters, we designed a table containing (i) all NK and monocytes subpopulations obtained by manual analysis; (ii) newborn clinical data; and (iii) 23 plasma cytokines. Pairwise correlations between variables were calculated and visualized as a correlogram using the corrplot R function, v0.84. Spearman's rank-correlation coefficient (ρ) was indicated by color scale; two-tailed p-value calculated using cor.mtest function of corrplot v0.84 was indicated by $*p < 0.05$, $**p < 0.01$, and $***p < 0.001$. All variables were displayed according to their original order without applying any hierarchical clustering. Single XY scatter plots were drawn using ggscatter function of ggpubr v0.4.0 package, reporting ρ and exact two-tailed p-value.

Data analysis and statistics

Quantitative variables, including age, clinical, and immunological parameters, were used for group comparisons, using both Kruskal–Wallis with original FDR method of Benjamini and Hochberg correction and GLMM, assuming nonparametric distribution. Correlations between clinical and molecular data were assessed using Spearman correlation. p Values < 0.05 were considered statistically significant. The figure reports data as mean values $\pm$ SEM. Statistical analyses were performed using Prism 7.0 (GraphPad Software, La Jolla, CA).

Conflict of interest: All authors declare no commercial or financial conflict of interest.

Ethics approval: This study was conducted in accordance with the Declaration of Helsinki and was approved by the local ethics committee (Prot# 2211/C.E.). All participants' parents signed written and informed consent.

Author contributions: A.N., R.B., and M.N. carried out experiments; S.D.B., A.N., and D.L.T. analyzed data; S.D.B. and A.C. wrote the paper and drafted the figures; E.M., L.Luc, L.Lug, L.G., F.M., L.B., E.B., A.B., I.N., F.Fer, and F.Fac enrolled the patients and collected clinical data; A.N. drafted the table; S.D.B. and A.C. supervised and conceived the study. All authors approved the manuscript.

Data availability statement: The data that support the findings of this study are available from the corresponding author upon reasonable request.

Peer review: The peer review history for this article is available at https://publons.com/publon/10.1002/eji.202250224

References

1 Busse, M., Redlich, A., Hartig, R., Costa, S. D., Rathert, H., Fest, S. and Zenclussen, A. C., Imbalance between inflammatory and regulatory cord blood B cells following pre-term birth. *J. Reprod. Immunol.* 2021. **145**: 103319.

2 Fang, X., Wang, Y., Zhang, Y., Li, Y., Kwak-Kim, J. and Wu, L., NLRP3 inflammasome and its critical role in gynecological disorders and obstetrical complications. *Front. Immunol.* 2020. **11**: 555826.

3 Liu, L., Oza, S., Hogan, D., Chu, Y., Perin, J., Zhu, J., Lawn, J. E. et al., Global, regional, and national causes of under-5 mortality in 2000–15: an updated systematic analysis with implications for the sustainable development goals. *Lancet* 2016. **388**: 3027–3035.

4 Walani, S. R., Global burden of preterm birth. *Int. J. Gynaecol. Obstet.* 2020. **150**: 31–33.

5 Altman, M., Vanpee, M., Cnattingius, S. and Norman, M., Moderately preterm infants and determinants of length of hospital stay. *Arch. Dis. Child. Fetal Neonatal Ed.* 2009. **94**: F414–418.

6 Berardi, A., Sforza, F., Baroni, L., Spada, C., Ambretti, S., Biasucci, G., Bolognesi, S. et al., Epidemiology and complications of late-onset sepsis: an Italian area-based study. *PLoS One* 2019. **14**: e0225407.

7 de Jong, E., Strunk, T., Burgner, D., Lavoie, P. M. and Currie, A., The phenotype and function of preterm infant monocytes: implications for susceptibility to infection. *J. Leukoc. Biol.* 2017. **102**: 645–656.

8 Tsafaras, G. P., Ntontsi, P. and Xanthou, G., Advantages and limitations of the neonatal immune system. *Front. Pediatr.* 2020. **8**: 5.

9 Yu, J. C., Khodadadi, H., Malik, A., Davidson, B., Salles, E., Bhatia, J., Hale, V. L. et al., Innate immunity of neonates and infants. *Front. Immunol.* 2018. **9**: 1759.

10 Zasada, M., Lenart, M., Rutkowska-Zapala, M., Stec, M., Mol, N., Czyz, O., Siedlar, M et al., Analysis of selected aspects of inflammasome function in the monocytes from neonates born extremely and very prematurely. *Immunobiology* 2018. **223**: 18–24.

11 Anderson, J., Thang, C. M., Thanh, L. Q., Dai, V. T. T., Phan, V. T., Nhu, B. T. H., Trang, D.N. X. et al., Immune profiling of cord blood from preterm and term infants reveals distinct differences in pro-inflammatory responses. *Front. Immunol.* 2021. **12**: 777927.

12 Perez, A., Gurbindo, M. D., Resino, S., Aguaron, A. and Munoz-Fernandez, M. A., NK cell increase in neonates from the preterm to the full-term period of gestation. *Neonatology* 2007. **92**: 158–163.

13 Ulas, T., Pirr, S., Fehlhaber, B., Bickes, M. S., Loof, T. G., Vogl, T., Mellinger, L et al., S100- alarmin-induced innate immune programming protects newborn infants from sepsis. *Nat. Immunol.* 2017. **18**: 622–632.

14 Kollmann, T. R., Kampmann, B., Mazmanian, S. K., Marchant, A. and Levy, O., Protecting the newborn and young infant from infectious diseases: lessons from immune ontogeny. *Immunity* 2017. **46**: 350–363.

15 Gibellini, L., De Biasi, S., Paolini, A., Borella, R., Boraldi, F., Mattioli, M., Lo Tartaro, D.et al., Altered bioenergetics and mitochondrial dysfunction of monocytes in patients with COVID-19 pneumonia. *EMBO Mol. Med.* 2020. **12**: e13001.

16 Maffei, R., Bulgarelli, J., Fiorcari, S., Bertoncelli, L., Martinelli, S., Guarnotta, C., Castelli, I. et al., The monocytic population in chronic lymphocytic leukemia shows altered composition and deregulation of genes involved in phagocytosis and inflammation. *Haematologica* 2013. **98**: 1115–1123.

17 Nasi, M., Pecorini, S., De Biasi, S., Bianchini, E., Digaetano, M., Neroni, A., Lo Tartaro, D. et al., Altered expression of PYCARD, interleukin 1beta, interleukin 18, and NAIP in successfully treated HIV-positive patients with a low ratio of CD4+ to CD8+ T cells. *J. Infect. Dis.* 2019. **219**: 1743–1748.

18 Khan, R. N. and Hay, D. P., A clear and present danger: inflammasomes DAMPing down disorders of pregnancy. *Hum. Reprod. Update* 2015. **21**: 388–405.

19 Liao, J., Kapadia, V. S., Brown, L. S., Cheong, N., Longoria, C., Mija, D., Ramgopal, M. et al., The NLRP3 inflammasome is critically involved in the development of bronchopulmonary dysplasia. *Nat. Commun.* 2015. **6**: 8977.

20 Stouch, A. N., McCoy, A. M., Greer, R. M., Lakhdari, O., Yull, F. E., Blackwell, T. S., Hoffman, H. M. et al., IL-1beta and inflammasome activity link inflammation to abnormal fetal airway development. *J. Immunol.* 2016. **196**: 3411–3420.

21 Chatterjee, P., Chiasson, V. L., Bounds, K. R. and Mitchell, B. M., Regulation of the anti- inflammatory cytokines interleukin-4 and interleukin-10 during pregnancy. *Front. Immunol.* 2014. **5**: 253.

22 Webster, N. L. and Crowe, S. M., Matrix metalloproteinases, their production by monocytes and macrophages and their potential role in HIV-related diseases. *J. Leukoc. Biol.* 2006. **80**: 1052–1066.

23 Cao, C., Gu, J. and Zhang, J., Soluble triggering receptor expressed on myeloid cell-1 (sTREM-1): a potential biomarker for the diagnosis of infectious diseases. *Front. Med.* 2017. **11**: 169–177.

24 Gomez-Pina, V., Soares-Schanoski, A., Rodriguez-Rojas, A., Del Fresno, C., Garcia, F., Vallejo-Cremades, M. T., Fernandez-Ruiz, I. et al., Metalloproteinases shed TREM-1 ectodomain from lipopolysaccharide-stimulated human monocytes. *J. Immunol.* 2007. **179**: 4065–4073.

25 Crowe, L. A. N., McLean, M., Kitson, S. M., Melchor, E. G., Patommel, K., Cao, H. M., Reilly, J. H. et al., S100A8 & S100A9: alarmin mediated inflammation in tendinopathy. *Sci. Rep.* 2019. **9**: 1463.

26 Lo Tartaro, D., Neroni, A., Paolini, A., Borella, R., Mattioli, M., Fidanza, L., Quong, A. et al., Molecular and cellular immune features of aged patients with severe COVID-19 pneumonia. *Commun. Biol.* 2022. **5**: 590.

27 Cossarizza, A., Chang, H. D., Radbruch, A., Acs, A., Adam, D., Adam-Klages, S., Agace, W. W. et al., Guidelines for the use of flow cytometry and cell sorting in immunological studies (second edition). *Eur. J. Immunol.* 2019. **49**: 1457–1973.

28 Poli, A., Michel, T., Theresine, M., Andres, E., Hentges, F. and Zimmer, J., CD56bright natural killer (NK) cells: an important NK cell subset. *Immunology* 2009. **126**: 458–465.

29 Gaddy, J. and Broxmeyer, H. E., Cord blood CD16+56- cells with low lytic activity are possible precursors of mature natural killer cells. *Cell. Immunol.* 1997. **180**: 132–142.

30 Gaddy, J., Risdon, G. and Broxmeyer, H. E., Cord blood natural killer cells are functionally and phenotypically immature but readily respond to interleukin-2 and interleukin-12. *J. Interferon Cytokine Res.* 1995. **15**: 527–536.

31 Alter, G., Teigen, N., Davis, B. T., Addo, M. M., Suscovich, T. J., Waring, M. T., Streeck, H. et al., Sequential deregulation of NK cell subset distribution and function starting in acute HIV-1 infection. *Blood* 2005. **106**: 3366–3369.

32 Mavilio, D., Lombardo, G., Benjamin, J., Kim, D., Follman, D., Marcenaro, E., O'Shea, M. A. et al., Characterization of CD56-/CD16+ natural killer (NK) cells: a highly dysfunctional NK subset expanded in HIV-infected viremic individuals. *Proc. Natl. Acad. Sci. USA.* 2005. **102**: 2886–2891.

33 De Maria, A., Bozzano, F., Cantoni, C. and Moretta, L., Revisiting human natural killer cell subset function revealed cytolytic CD56(dim)CD16+ NK cells as rapid producers of abundant IFN-gamma on activation. *Proc. Natl. Acad. Sci. USA.* 2011. **108**: 728–732.

34 Riva, G., Castellano, S., Nasillo, V., Ottomano, A. M., Bergonzini, G., Paolini, A., Lusenti, B. et al., Monocyte distribution width (MDW) as novel inflammatory marker with prognostic significance in COVID-19 patients. *Sci. Rep.* 2021. **11**: 12716.

35 Nakamori, Y., Park, E. J. and Shimaoka, M., Immune deregulation in sepsis and septic shock: reversing immune paralysis by targeting PD-1/PD-L1 pathway. *Front. Immunol.* 2020. **11**: 624279.

36 Huang, Y., Xu, W. and Zhou, R., NLRP3 inflammasome activation and cell death. *Cell. Mol. Immunol.* 2021. **18**: 2114–2127.

37 Paolini, A., Borella, R., De Biasi, S., Neroni, A., Mattioli, M., Lo Tartaro, D., Simonini, C. et al., Cell death in coronavirus infections: uncovering its role during COVID-19. *Cells* 2021. **10**: 1585.

38 Bauer, R. and Rauch, I., The NAIP/NLRC4 inflammasome in infection and pathology. *Mol. Aspects Med.* 2020. **76**: 100863.

39 Kumari, P., Russo, A. J., Shivcharan, S. and Rathinam, V. A., AIM2 in health and disease: inflammasome and beyond. *Immunol. Rev.* 2020. **297**: 83–95.

40 Kay, C., Wang, R., Kirkby, M. and Man, S. M., Molecular mechanisms activating the NAIP- NLRC4 inflammasome: implications in infectious disease, autoinflammation, and cancer. *Immunol. Rev.* 2020. **297**: 67–82.

41 Yang, Han, Z. and Oppenheim, J. J., Alarmins and immunity. *Immunol. Rev.* 2017. **280**: 41–56.

42 Vogl, T., Tenbrock, K., Ludwig, S., Leukert, N., Ehrhardt, C., van Zoelen, M. A., Nacken, W. et al., Mrp8 and Mrp14 are endogenous activators of Toll-like receptor 4, promoting lethal, endotoxin-induced shock. *Nat. Med.* 2007. **13**: 1042–1049.

43 Schelbergen, R. F., Geven, E. J., van den Bosch, M. H., Eriksson, H., Leanderson, T., Vogl, T., Roth, J. et al., Prophylactic treatment with S100A9

inhibitor paquinimod reduces pathology in experimental collagenase-induced osteoarthritis. *Ann. Rheum. Dis.* 2015. **74**: 2254–2258.

44 **Pacora, P., Romero, R., Maymon, E., Gervasi, M. T., Gomez, R., Edwin, S. S. and Yoon, B. H.**, Participation of the novel cytokine interleukin 18 in the host response to intra-amniotic infection. *Am. J. Obstet. Gynecol.* 2000. **183**: 1138–1143.

45 **Reddy, P.**, Interleukin-18: recent advances. *Curr. Opin. Hematol.* 2004. **11**: 405–410.

46 **Ekelund, C. K., Vogel, I., Skogstrand, K., Thorsen, P., Hougaard, D. M., Langhoff-Roos, J. and Jacobsson, B.**, Interleukin-18 and interleukin-12 in maternal serum and spontaneous preterm delivery. *J. Reprod. Immunol.* 2008. **77**: 179–185.

47 **Koscica, K. L., Ananth, C. V., Placido, J. and Reznik, S. E.**, The effect of a matrix metalloproteinase inhibitor on inflammation-mediated preterm delivery. *Am. J. Obstet. Gynecol.* 2007. **196**: 551 e551–553.

48 **De Biasi, S., Meschiari, M., Gibellini, L., Bellinazzi, C., Borella, R., Fidanza, L., Gozzi, L. et al.**, Marked T cell activation, senescence, exhaustion and skewing towards TH17 in patients with COVID-19 pneumonia. *Nat. Commun.* 2020. **11**: 3434.

49 **Nowicka, M., Krieg, C., Crowell HL., Weber, L. M., Hartmann, F. J., Guglietta, S., Becher, B. et al.**, CyTOF workflow: differential discovery in high-throughput high-dimensional cytometry datasets. *F1000Research* 2019. **6**: 748.

Abbreviations: **CB**: cord blood · **CBMC**: CB mononuclear cell · **DAMP**: damage-associated molecular pattern

Full correspondence: Dr. Sara De Biasi, Department of Medical and Surgical Sciences for Children & Adults, University of Modena and Reggio Emilia, Via Campi, 287, 41125 Modena, Italy
e-mail: sara.debiasi@unimore.it